Hydride-ion-conducting K_2NiF_4-type Ba–Li oxyhydride solid electrolyte

Fumitaka Takeiri[1,2,10], Akihiro Watanabe[1,3,10], Kei Okamoto[1,2], Dominic Bresser[4,5,6], Sandrine Lyonnard[4], Bernhard Frick[7], Asad Ali[1,2], Yumiko Imai[1], Masako Nishikawa[1], Masao Yonemura[2,8], Takashi Saito[2,8], Kazutaka Ikeda[2,8], Toshiya Otomo[2,8], Takashi Kamiyama[2,8], Ryoji Kanno[3,9] and Genki Kobayashi[1,2] ✉

Hydrogen transport in solids, applied in electrochemical devices such as fuel cells and electrolysis cells, is key to sustainable energy societies. Although using proton (H^+) conductors is an attractive choice, practical conductivity at intermediate temperatures (200–400 °C), which would be ideal for most energy and chemical conversion applications, remains a challenge. Alternatively, hydride ions (H^-), that is, monovalent anions with high polarizability, can be considered a promising charge carrier that facilitates fast ionic conduction in solids. Here, we report a K_2NiF_4-type Ba–Li oxyhydride with an appreciable amount of hydrogen vacancies that presents long-range order at room temperature. Increasing the temperature results in the disappearance of the vacancy ordering, triggering a high and essentially temperature-independent H^- conductivity of more than 0.01 S cm^{-1} above 315 °C. Such a remarkable H^- conducting nature at intermediate temperatures is anticipated to be important for energy and chemical conversion devices.

Hydrogen transport in solids has received considerable attention owing to its potential for electrochemical devices, such as fuel cells, electrolysis cells, gas separation membranes and chemical conversion processes. In particular, materials conducting hydrogen in the form of protons (H^+), that is, proton conductors such as oxides[1], solid acids[2,3] and polymers[4,5], have been investigated extensively to this end. Among them, water-containing materials (acids, polymers and hydrates) are good conductors below their decomposition or dehydration point, which is 200 °C at most, while oxide materials, represented by perovskites such as $BaCeO_3$ (ref. [6]) and $BaZrO_3$ (ref. [7]), require higher temperatures, above ~500 °C, to induce OH dipole reorientation and proton hopping (that is, OH hydrogen bond cleavage). The development of proton conductors is progressing steadily; however, fast hydrogen transport in solids at intermediate temperatures of 200–400 °C, at which various crucial chemical and energy conversion processes take place, remains a challenge[8].

The hydride ion (H^-) possesses low charge density due to its moderate ionic radius despite having the lowest mass number, in contrast to the extremely high charge density of protons, and consequently has high polarizability. This basic characteristic is favourable for fast ion conduction in general and also in solids[9]. In fact, metal hydride BaH_2 exhibits a remarkable ionic conductivity of 0.2 S cm^{-1} at 630 °C, which is higher than those of typical good O^{2-} and H^+ conducting oxides, such as stabilized zirconia and the barium cerate series[10]. We previously reported H^- conduction in a typically rigid oxide-based framework by finding a series of layered perovskite (K_2NiF_4-type) $La_{2-x-y}Sr_{x+y}LiH_{1-x+y}O_{3-y}$ (ref. [11]). This discovery triggered the exploration of H^--conducting oxyhydrides, for example the isostructural Ln_2LiHO_3 (Ln = Pr, Nd)[12], $LnSrLiH_2O_2$ (Ln = Pr, Nd, Sm, Gd)[13], Ba_2MHO_3 (M = Sc, Y)[14,15] and fluorite-type $LaH_{3-2x}O_x$ (refs. [16,17]). However, a H^- conductor exhibiting both high conductivity and low activation energy has not been developed yet, to the best of our knowledge. The activation energies reported for oxyhydrides range between 68 and 125 kJ mol^{-1}, which is somewhat larger than expected from the H^- character mentioned above. Here, we report on a K_2NiF_4-type oxyhydride, consisting of barium and lithium cations, that exhibits both a high H^- conductivity of >0.01 S cm^{-1} and an extremely low activation energy above 315 °C.

Polycrystalline samples of Ba–Li oxyhydrides were synthesized by two different solid-state reactions. In one case, a mixture of BaH_2, BaO and LiH was sintered at 650 °C and 2 GPa using a cubic anvil-type cell (high-pressure synthesis), while in the other case, the same mixture was sintered in a stainless steel tube filled with H_2 gas (ambient-pressure synthesis). Room-temperature synchrotron X-ray diffraction (SXRD) revealed that the sample obtained by the high-pressure synthesis adopts a tetragonal unit cell (*I*4/*mmm* space group; no. 139) with $a = 3.95974(3)$ Å and $c = 14.20850(14)$ Å (Supplementary Fig. 1a). Refinement of the neutron diffraction (ND) profile (Fig. 1a and Supplementary Table 1) revealed a partially anion-ordered K_2NiF_4-type structure in which the equatorial sites are occupied by only H atoms and H/O are randomly distributed at the apical sites, as is also the case for the isostructural Sr_2LiH_3O (ref. [11]; Fig. 1b). This phase is hereafter referred to as α-BLHO. The refined composition of $Ba_2LiH_{2.775(2)}O_{1.153(1)}$ slightly deviates from the stoichiometric Ba_2LiH_3O, with 15% excess O at the apical sites and 7.5% vacancies at the equatorial sites. The tendency

[1]Department of Materials Molecular Science, Institute for Molecular Science, Okazaki, Japan. [2]The Graduate University for Advanced Studies, SOKENDAI, Hayama, Japan. [3]Department of Chemical Science and Engineering, School of Materials and Chemical Technology, Tokyo Institute of Technology, Midori, Japan. [4]Université Grenoble Alpes, CEA, CNRS, IRIG, SyMMES, Grenoble, France. [5]Helmholtz Institute Ulm, Ulm, Germany. [6]Karlsruhe Institute of Technology, Karlsruhe, Germany. [7]Institut Laue-Langevin (ILL), Grenoble, France. [8]Institute of Materials Structure Science, High Energy Accelerator Research Organization (KEK), Ibaraki, Japan. [9]Research Center for All-Solid-State Battery, Institute of Innovative Research, Tokyo Institute of Technology, Yokohama, Japan. [10]These authors contributed equally: Fumitaka Takeiri, Akihiro Watanabe. ✉e-mail: gkobayashi@ims.ac.jp

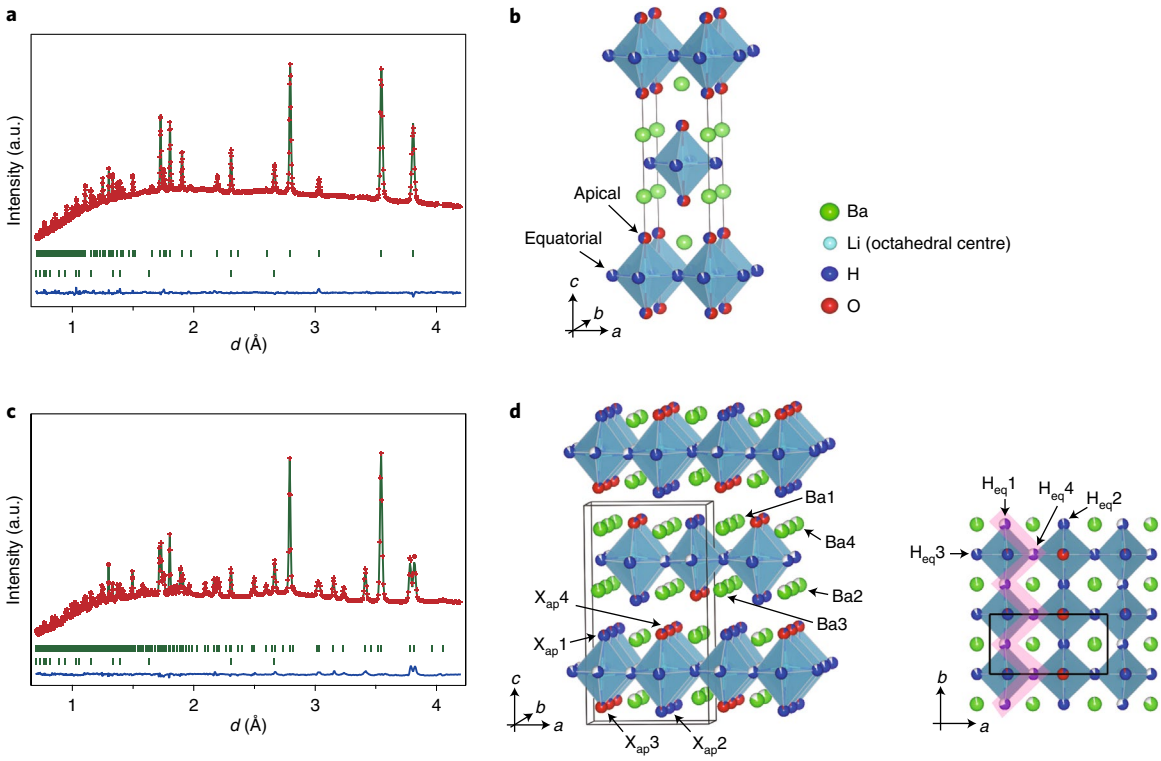

Fig. 1 | Crystal structures of as-synthesized K_2NiF_4-type oxyhydrides at room temperature. a,**b**, Refinement profile of ND (**a**) and refined structure of $Ba_2LiH_{2.8}O_{1.1}$ (**b**) prepared by high-pressure synthesis. **c**,**d**, Refinement profile of ND (**c**) and refined structure of $Ba_{1.75}LiH_{2.7}O_{0.9}$ (**d**) prepared by ambient-pressure synthesis. In the profiles, the red crosses and green solid curves represent observed and calculated intensities, respectively. The blue solid lines at the bottom indicate residual curves. The upper and lower green ticks indicate the peak positions of oxyhydride and Li_2O, respectively.

for the vacancies to preferentially occupy the equatorial sites is consistent with the structures of other Li-based oxyhydrides[11].

The room-temperature SXRD pattern of the sample obtained via ambient-pressure synthesis (Supplementary Fig. 1b) was apparently similar to that of α-BLHO, but the lattice symmetry was lowered, being orthorhombic with $a = 7.92577(3)$ Å, $b = 3.92294(1)$ Å and $c = 14.15820(6)$ Å, which is close to a $2\times1\times1$ expanded unit cell of α-BLHO. A fit of the ND profile to a structural model based on the $Pnm2_1$ (no. 31) space group converged reasonably (Fig. 1c and Supplementary Table 2), resulting in a structure with the composition $Ba_{1.75(1)}LiH_{2.67(2)}O_{0.935(6)}$, hereafter called β-BLHO. This structure is presented in Fig. 1d, along with labels illustrating the notation used to describe the atomic sites. The charge neutrality is maintained by the simultaneous introduction of Ba and anion vacancies, suggesting that the β-phase contains Schottky-like deficiencies ($Ba_{2-x-y}LiH_{3-2x}O_{1-y}$; $x \approx 0.15$, $y \approx 0.1$) in which vacancies are introduced by removal of $x$$BaH_2$ and yBaO from stoichiometric Ba_2LiH_3O. Such a sizable quantity of vacancies at the barium and anion sites contributes to the formation of long-range order along the *a* direction in β-BLHO: for Ba, a strip of less-vacant (Ba1, Ba3) sites and more-vacant (Ba2, Ba4) sites; for O, alternate filling of the apical ($X_{ap}3$, $X_{ap}4$) sites (X_{ap} represents a H or O element at apical sites); and for H at the equatorial sites, a zigzag strip of more-vacant ($H_{eq}1$, $H_{eq}4$) sites and less-vacant ($H_{eq}2$, $H_{eq}3$) sites in the *ab* plane. The absence of hydroxyl groups in the prepared sample was confirmed by Fourier transform infrared spectroscopy (Supplementary Fig. 2).

The observed difference in structure depending on the synthesis conditions indicates that α-BLHO is metastable at ambient pressure. Indeed, the SXRD patterns of the tetragonal phase at elevated temperatures (Supplementary Fig. 3) revealed a transformation to an orthorhombic phase together with the appearance of a sizable quantity of BaO, which indicates the formation of the β-phase through its thermal extraction. The extracted BaO remained in the sample after cooling to room temperature, meaning that this transformation is an irreversible reaction.

Temperature-controlled SXRD experiments were also performed for β-BLHO prepared by ambient-pressure synthesis, as plotted in Fig. 2a. Upon heating, the $2\times1\times1$ orthorhombic supercell transformed into a simple $1\times1\times1$ K_2NiF_4-type tetragonal cell (space group, $I4/mmm$; $a = 3.97899(5)$ Å, $c = 14.2849(5)$ Å at 400 °C), suggesting that the above-described ordering in β-BLHO has completely disappeared. The temperature dependence of the lattice constants (Fig. 2b) indicates that, for the *a* and *b* axes, inflection and integration points exist at 300 °C and 360 °C, respectively. In the cooling process, a reversible transition was observed without any evolution of impurities, indicating that there was no change in composition up to 400 °C.

To clarify the phase transition, temperature-controlled ND measurements were carried out at 263–368 °C. Details of the refinements for each temperature are given in Supplementary Discussion 1, Supplementary Figs. 4 and 5 and Supplementary Tables 3 and 4. At 263 and 300 °C, almost the same atomic distribution as in the β-phase was observed, where the above-mentioned three types of orderings, namely H_{eq}/V_H, H_{ap}/O_{ap} and Ba/V_{Ba} (H_{eq} and V_M represent a hydrogen at equatorial sites and a vacancy at an M site, respectively) were retained (Fig. 2c, left). By contrast, at 314, 325 and 343 °C, the structures converged with the higher-symmetry orthorhombic structures (space group, *Pnma* (no. 62)) in which the H_{eq}/V_H and Ba/V_{Ba} ordering disappeared, but the H_{ap}/O_{ap} ordering remained (Fig. 2c, centre, hereafter called γ-BLHO). At higher temperatures, at 350 and 368 °C, the profile could be indexed as a simple tetragonal K_2NiF_4-type structure (space group, $I4/mmm$),

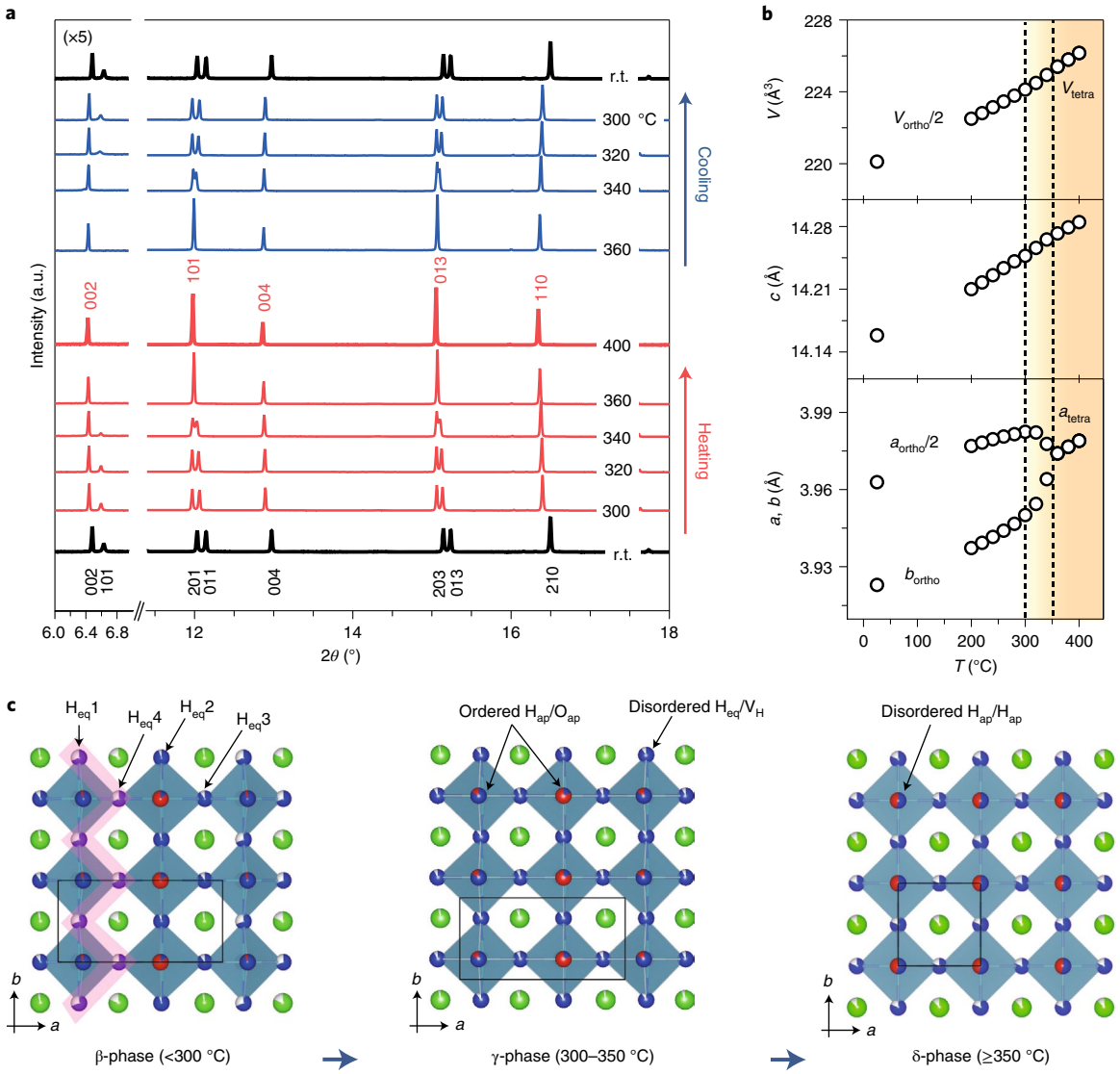

Fig. 2 | Structural phase transition of $Ba_{1.75}LiH_{2.7}O_{0.9}$ prepared by ambient-pressure synthesis. a, Temperature-controlled SXRD patterns. The black and red *hkl* indices correspond to the orthorhombic and tetragonal unit cells, respectively. The low-angle region exhibits the appearance and disappearance of the orthorhombic (101) reflection. r.t., room temperature. **b**, Temperature dependence of the unit cell parameters. V represents a cell volume. Subscripts ortho and tetra represent orthorhombic (<350 ºC) and tetragonal (≥350 ºC) cells, respectively. Dashed line highlights the phase transition points. **c**, Proposed heating-induced phase transition. Crystal structures for each phase projected along the *c*-axis are compared. The green, blue and red balls represent Ba, H and O atoms, respectively. The highlight of the β-BLHO is the region where H^- vacancies are localized.

as shown in Fig. 2c (right, called δ-BLHO), in which the ordering completely disappeared. To summarize the powder diffraction studies, β-BLHO should exhibit successive phase transitions at around 300 and 350 °C; these transitions were also detected via differential scanning calorimetry measurements upon heating (Supplementary Fig. 6).

The conduction properties for β-BLHO prepared by ambient-pressure synthesis were investigated by electrochemical impedance spectroscopy in the temperature range $200 \leq T \leq 350$ °C. Below 300 °C, the spectra take the form of broad semicircles in the high-frequency range, as seen in Fig. 3a (inset); these spectral signals can be separated into bulk and grain boundary contributions and the electrode response in the low-frequency range. The electrode response depends on the H_2-blocking Mo (Fig. 3a) and transparent Pd (Supplementary Fig. 7) materials, indicating that a hydrogen species serves as charge carrier. Above 300 °C, the resistance decreases drastically, and the total conductivity, that is, the bulk and grain boundary contributions, could be estimated from the intercept of the spike. The temperature dependence of the conductivity for BLHO (Fig. 3b) shows a drastic jump at around 300 °C, which should correspond to the initial (β–γ) phase transition point, that is, to the disordering of H_{eq}/V_H. The conductivity increased by three orders of magnitude at that point and reached a remarkably high value, over 1×10^{-2} S cm^{-1}, above 315 °C. The electromotive force values obtained at 350 °C by a hydrogen concentration cell, exhibiting a hydrogen partial pressure dependence according to the Nernst equation (Supplementary Discussion 2 and Supplementary Fig. 8), support that H^-, rather than H^+ or electrons (e^-), is the dominant charge carrier.

Such a drastic increase in ionic conductivity accompanied with an order–disorder phase transition has an analogy with a well-known oxide ion conductor, $Ba_2In_2O_5$, in which the conductivity is enhanced through the phase transition from the orthorhombic brownmillerite to the cubic perovskite at ~930 °C (ref. [18]). However,

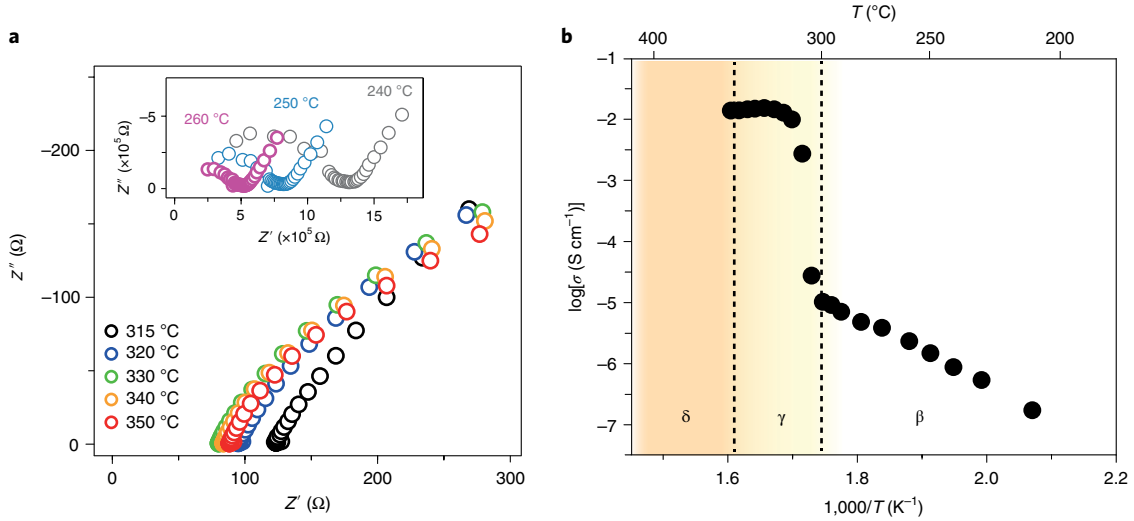

Fig. 3 | Hydride conductivity of $Ba_{1.75}LiH_{2.7}O_{0.9}$. **a**, Impedance spectra at 315-350 and 240-260 ºC (inset). The data presented in the form of imaginary, Z'' (capacitive), against real, Z' (resistive), impedances. **b**, Arrhenius plot on the H^- conductivity (σ) estimated from the impedance data.

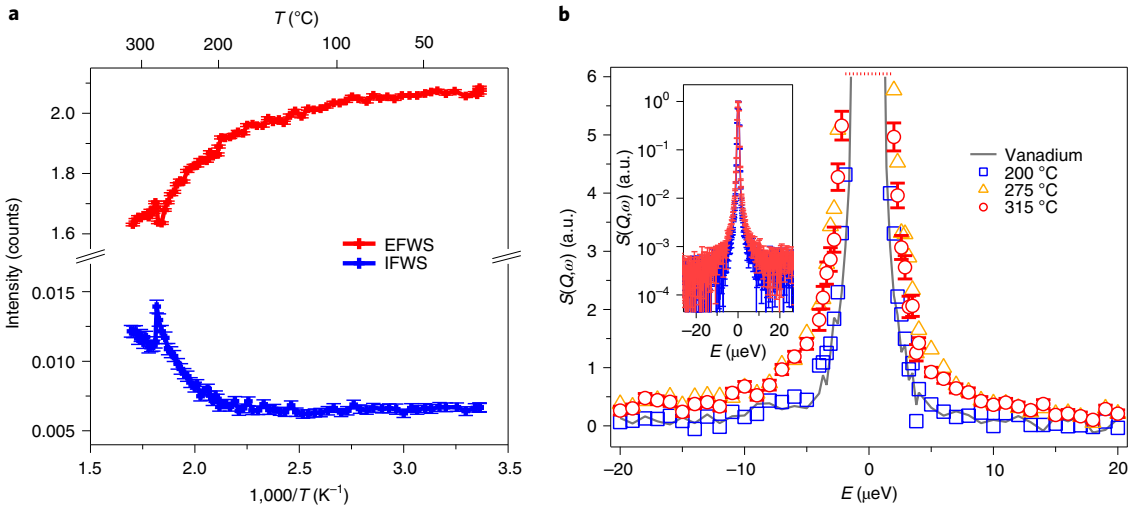

Fig. 4 | Molecular-level H^- dynamics. **a**, EFWS and IFWS acquired in heating mode for averaged Q range. **b**, Expanded and entire (inset) Q-averaged QENS spectra acquired at 200 °C (blue), 275 °C (orange) and 315 °C (red), compared with that from a vanadium cell (grey line). The data are summed over all Q values, where Q is the momentum transfer. For clarity, the error bars are only shown in the expanded figure for the highest temperature.

for BLHO, the slope of the Arrhenius plot, that is, the activation energy E_a, decreases drastically after the β–γ phase transition, which is critically different from $Ba_2In_2O_5$. This conducting behaviour in BLHO indicates that the β–γ phase transition totally changed the H^- diffusion mechanism from the simple ion hopping via anion vacancies proposed in the previous theoretical studies on K_2NiF_4-type Li-based oxyhydrides[12,19,20]. Note that a slight decrease in conductivity above 330 °C (Fig. 3a) might be related to the γ–δ transition (Supplementary Discussion 3 and Supplementary Fig. 9).

To investigate the molecular-scale motions of H^- in BLHO, we carried out quasi-elastic neutron scattering (QENS), wherein the dynamics of hydrogen can be prominently detected due to its large incoherent scattering cross-section. Figure 4a shows the temperature dependence of the elastic and inelastic fixed-window scans (EFWS and IFWS, respectively; details are given in Supplementary Discussion 4.1 and Supplementary Fig. 10). Below 200 °C, the EFWS intensity decreased with a temperature increase of the Debye–Waller factor, and it dropped more sharply above 200 °C, suggesting the activation of a dynamic process. The increase of the IFWS intensity at an energy transfer of 2 μeV in the same temperature range supports the assumption that a dynamic process on a timescale shorter than a few nanoseconds entered the time window of the spectrometer. These observations indicate a gradual acceleration of H^- motion with temperature. Moreover, in both elastic and inelastic signals, sharp anomalies that correspond to the β–γ phase transition involving the Ba/V_{Ba} and H_{eq}/V_H disorders were observed at around 275 °C. This temperature is slightly lower than the phase boundary point determined by diffraction results; this result is reasonable, considering the fact that mainly local hydrogen motion was detected by EFWS and IFWS.

Based on the results, QENS spectra were collected at 200, 275 and 315 °C (Supplementary Fig. 10). The total scattering intensities $S(\omega)$, i.e. averaged over the available momentum transfer (Q) range, are plotted in Fig. 4b against the energy transfer ($E = \hbar\omega$), where $\hbar$ and ω represent Dirac's constant and angular frequency, respectively. In contrast to the data at 200 °C, where

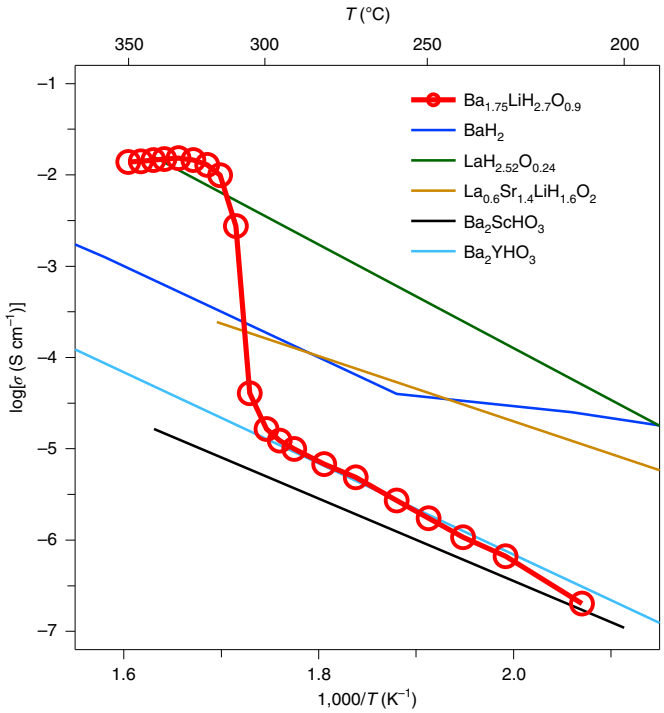

Fig. 5 | Comparison of H^- conductivities of $Ba_{1.75}LiH_{2.7}O_{0.9}$ and other materials. Shown are H^- conductors: BaH_2 (ref. [10]), $La_{0.6}Sr_{1.4}LiH_{1.6}O_2$ (ref. [11]), Ba_2ScHO_3 (ref. [14]), Ba_2YHO_3 (ref. [15]) and $LaH_{2.52}O_{0.24}$ (ref. [16]).

$S(\omega)$ contains only an intense elastic peak, the high-temperature data at 275 and 315 °C exhibit a clear quasi-elastic signal, indicating notably facilitated H^- diffusion at the higher temperatures. We performed an approximate estimation of the self-diffusion coefficient of hydrogen (D_H) at 315 °C by fitting the Q dependence of the quasi-elastic components, yielding reasonable values ($\sigma \approx 10^{-2}$ S cm^{-1}), similar to the conductivity estimated by electrochemical impedance spectroscopy; these results support that the observed high conductivities in γ-BLHO are attributed to hydrogen motion (Supplementary Discussion 4.2 and Supplementary Figs. 11–14). Interestingly, the QENS signal at 315 °C hardly changed from that at 275 °C, meaning almost unchanged D_H above 275 °C. This fact implies that the local H^- mobility is already activated at 275 °C and the β–γ transition allows for its long-range diffusion, that is, high H^-conductivity.

Finally, the conduction behaviour of BLHO is compared with representative H^- conductors[10,11,14–16], as shown in Fig. 5. The conductivity of BLHO after the β–γ transition is comparable to that of $LaH_{3-2x}O_x$ (ref. [16]), which exhibits the highest conductivity at around 300 °C. In addition, a notably low activation energy has not been reported in H^- conductors including BaH_2 (50 kJ mol^{-1})[10], $La_{2-x-y}Sr_{x+y}LiH_{1-x+y}O_{3-y}$ (64–95 kJ mol^{-1})[11] and $LaH_{3-2x}O_x$ (116–125 kJ mol^{-1})[16]. Such an ion-conducting behaviour is characteristic in so-called superionic conductors represented by $RbAg_4I_5$ (refs. [21,22]), $Rb_4Cu_{16}I_7Cl_{13}$ (ref. [23]), $PbSnF_4$ (ref. [24]) and $Li_{10}GeP_2S_{12}$ (ref. [25]), suggesting a possible occurrence of a H^- superionic conduction state in the γ- and δ-phases of BLHO.

Conclusions

In this study, we synthesized a K_2NiF_4-type Ba–Li oxyhydride (BLHO) by ambient and high-pressure reactions and showed that the highly vacant $Ba_{2-x-y}LiH_{3-2x}O_{1-y}$ ($x \approx 0.15$, $y \approx 0.1$; β-BLHO) is a stable phase under ambient pressure. SXRD and ND studies showed that the β-phase has long-range orderings in H_{eq}/V_H, H_{ap}/O_{ap} and Ba/V_{Ba} sites that are successively disordered upon heating to form the high-temperature phases (γ- and δ-phases). Electrochemical measurements revealed that the β–γ transition in BLHO at around 300 °C induces high and almost temperature-independent H^- conductivity, a result that is supported by the hydrogen dynamics detected via QENS. For BLHO with a perovskite-related structure, there is ample room for further optimization, for example, by substituting specific elements at both the cationic and anionic sites. Stabilizing the high-temperature phases of BLHO would be a principal strategy for the electrochemical use of H^- in the intermediate temperature range.

References

1. Kreuer, K. D. Proton-conducting oxides. *Annu. Rev. Mater. Res.* **33**, 333–359 (2003).
2. Haile, S. M., Boysen, D. A., Chisholm, C. R. I. & Merle, R. B. Solid acids as fuel cell electrolytes. *Nature* **410**, 910–913 (2001).
3. Hogarth, W. H. J., Diniz da Costa, J. C. & Lu, G. Q. Solid acid membranes for high temperature (>140°C) proton exchange membrane fuel cells. *J. Power Sources* **142**, 223–237 (2005).
4. Li, Q., He, R., Jensen, J. O. & Bjerrum, N. J. Approaches and recent development of polymer electrolyte membranes for fuel cells operating above 100 °C. *Chem. Mater.* **15**, 4896–4915 (2003).
5. Kreuer, K. D. On the development of proton conducting polymer membranes for hydrogen and methanol fuel cells. *J. Membr. Sci.* **185**, 29–39 (2001).
6. Iwahara, H., Uchida, H., Ono, K. & Ogaki, K. Proton conduction in sintered oxides based on $BaCeO_3$. *J. Electrochem. Soc.* **135**, 529–533 (1988).
7. Tao, S. & Irvine, J. T. S. Conductivity studies of dense yttrium-doped $BaZrO_3$ sintered at 1325°C. *J. Solid State Chem.* **180**, 3493–3503 (2007).
8. Norby, T. Solid-state protonic conductors: principles, properties, progress and prospects. *Solid State Ion.* **125**, 1–11 (1999).
9. Yamaguchi, S. Large, soft, and polarizable hydride ions sneak around in an oxyhydride. *Science* **351**, 1262–1263 (2016).
10. Verbraeken, M. C., Cheung, C., Suard, E. & Irvine, J. T. S. High H^- ionic conductivity in barium hydride. *Nat. Mater.* **14**, 95–100 (2015).
11. Kobayashi, G. et al. Pure H^- conduction in oxyhydrides. *Science* **351**, 1314–1317 (2016).
12. Iwasaki, Y. et al. Synthesis, crystal structure, and ionic conductivity of hydride ion-conducting Ln_2LiHO_3 (Ln = La, Pr, Nd) oxyhydrides. *J. Mater. Chem. A* **6**, 23457–23463 (2018).
13. Matsui, N. et al. The effect of cation size on hydride-ion conduction in $LnSrLiH_2O_2$ (Ln = La, Pr, Nd, Sm, Gd) oxyhydrides. *J. Mater. Chem. A* **8**, 24685–24694 (2020).
14. Takeiri, F. et al. Ba_2ScHO_3: H^- conductive layered oxyhydride with H^- site selectivity. *Inorg. Chem.* **58**, 4431–4436 (2019).
15. Nawaz, H., Takeiri, F., Kuwabara, A., Yonemura, M. & Kobayashi, G. Synthesis and H^- conductivity of a new oxyhydride Ba_2YHO_3 with anion-ordered rock-salt layers. *Chem. Commun.* **56**, 10373–10376 (2020).
16. Fukui, K. et al. Characteristic fast H^- ion conduction in oxygen-substituted lanthanum hydride. *Nat. Commun.* **10**, 2578 (2019).
17. Ubukata, H. et al. Hydride conductivity in an anion-ordered fluorite structure LnHO with an enlarged bottleneck. *Chem. Mater.* **31**, 7360–7366 (2019).
18. Goodenough, J. B., Ruiz-Diaz, J. E. & Zhen, Y. S. Oxide-ion conduction in $Ba_2In_2O_5$ and $Ba_3In_2MO_8$ (M=Ce, Hf, or Zr). *Solid State Ion.* **44**, 21–31 (1990).
19. Fjellvåg, Ø. S., Armstrong, J., Vajeeston, P. & Sjåstad, A. O. New insights into hydride bonding, dynamics, and migration in La_2LiHO_3 oxyhydride. *J. Phys. Chem. Lett.* **9**, 353–358 (2018).
20. Liu, X., Bjorheim, T. S. & Haugsrud, R. Formation of defects and their effects on hydride ion transport properties in a series of K_2NiF_4-type oxyhydrides. *J. Mater. Chem. A* **6**, 1454–1461 (2018).
21. Owens, B. B. & Argue, G. R. High-conductivity solid electrolytes: MAg_4I_5. *Science* **157**, 308–310 (1967).
22. Bradley, J. N. & Greene, P. D. Solids with high ionic conductivity in group 1 halide systems. *Trans. Faraday Soc.* **63**, 424–430 (1967).

23. Takahashi, T., Yamamoto, O., Yamada, S. & Hayashi, S. Solid-state ionics: high copper ion conductivity of the system CuCl - CuI - RbCl. *J. Electrochem. Soc.* **126**, 1654 (1979).
24. Dénès, G., Milova, G., Madamba, M. C. & Perfiliev, M. Structure and ionic transport of $PbSnF_4$ superionic conductor. *Solid State Ion.* **86-88**, 77–82 (1996).
25. Kamaya, N. et al. A lithium superionic conductor. *Nat. Mater.* **10**, 682–686 (2011).

Methods

Powder samples of Ba_2LiH_3O were synthesized by a conventional solid-state reaction under ambient and high-pressure conditions. The starting reagents, BaH_2 (Mitsuwa Chemical, 99.5%), BaO (Aldrich, 99.99%) and LiH (Alfa Aesar, 99.4%), were thoroughly mixed by planetary ball-milling for 3 h under an Ar atmosphere. In the ambient-pressure synthesis, the mixture was pelletized and encapsulated in a SUS sintering container designed in our previous work[26], filled with H_2 gas at a pressure of 0.2 MPa, followed by sintering at 650 °C for 6 h. In the high-pressure synthesis, the pelletized mixture was set in a cubic anvil cell and sintered at 650 °C at a pressure of 2 GPa. The sample preparation, except for the sintering process, and storage were done in the Ar-filled glove box ($H_2O < 0.2$ ppm) to avoid the sample coming into contact with moisture.

High-resolution SXRD experiments were performed at the SPring-8 BL02B2 beamline equipped with MYTHEN solid-state detectors[27], using an incident beam monochromatized to a wavelength $\lambda = 0.8$ Å. The well-ground powder sample was loaded into a capillary (0.3 mm in diameter). The capillary was rotated during measurements for better averaging of the powder pattern data. Time-of-flight ND experiments were carried out at room temperature and high temperature using SPICA and NOVA diffractometers, respectively, at the Japan Proton Accelerator Research Complex (J-PARC) facility, with approximately 1 g of powder samples loaded in vanadium cells (6 mm radius, 55 mm height). The obtained SXRD and ND data were analysed using the RIETAN-FP[28] and Z-Rietveld[29] programs, respectively. Crystal structures were illustrated by the VESTA program[30].

Infrared spectra were recorded using a Bruker ALPHA Fourier transform infrared spectrometer equipped with a single-reflection diamond attenuated total reflectance module. The spectrometer was set up in the Ar-filled glove box. Lithium hydroxide (LiOH, Tokyo Chemical Industry, 98.0%) was used as a reference sample. Differential scanning calorimetry measurements were carried out with a Rigaku DSC8231 instrument. A powder sample of β-BLHO was placed in a crimped stainless steel pan and heated to 400 °C before being cooled to 50 °C at a rate of 10 °C min^{-1} under Ar gas.

QENS was performed by using the IN16B neutron backscattering spectrometer at the Institute Laue-Langevin (ILL) in Grenoble, France[31,32]. For the IN16B measurements, a neutron wavelength of $\lambda = 6.271$ Å was selected, which corresponds to a resolution of 0.8 μeV (full width at half-maximum). The wavevector transfer Q available with this setting ranged from 0.2 to 1.9 Å. Two types of measurements were performed using the IN16B instrument. First, in heating from 24.15 to 314.5 °C at a rate of 3–5 °C min^{-1}, we recorded the elastic intensity (EFWS at energy transfer $\hbar\omega = 0$) alternating with the inelastic intensity (IFWS at a chosen energy of $\hbar\omega = 2$ μeV)[33]. These fixed-window temperature scans were then interrupted at three selected temperatures (200, 275 and 315 °C) to acquire full quasi-elastic spectra over a dynamical range of ±30 μeV, using a Doppler drive to change the wavelength of the incident neutrons. The samples, having a thickness of 0.2 mm, were investigated in an aluminium hollow-cylinder holder. Details on the technique and data analysis are given in Supplementary Discussion 4.

Electrochemical measurements were carried with sintered pellets of $Ba_{1.75}LiH_{2.7}O_{0.9}$ (10 mm in diameter) prepared under ambient pressure. Molybdenum or palladium electrodes for both sides of the cell were fabricated by magnetron sputtering. Ionic conductivity was measured via a.c. impedance methods with an applied voltage of 50 mV in the frequency range 35 MHz–0.1 Hz using a Bio-Logic MTZ-35 frequency response analyser. The measurements were performed in a flow of G1-grade H_2 gas (>99.99999 vol%) passed through a moisture trap (Agilent Big Moisture Trap BMT-4). Electromotive force values for hydrogen concentration cells constructed as (fixed hydrogen partial pressure $P_{H2} = 1$ atm) Pd|Ti|$Ba_{1.75}LiH_{2.7}O_{0.9}$|Ti|Pd (the varied P'_{H2}) were recorded by changing the hydrogen partial pressure P'_{H2} from 0.1 to 1.0 atm. The measurement temperature was fixed at 350 °C, at which $Ba_{1.75}LiH_{2.7}O_{0.9}$ shows superionic conduction. Thermiculite (Flexitallic) was used as a sealing material, and the voltage for each P'_{H2} value was recorded on a Bio-Logic VSP-300.

Data availability

The data presented in the current study are available from the corresponding author on reasonable request. Source data are provided with this paper.

References

26. Watanabe, A. et al. Ambient pressure synthesis and H^- conductivity of $LaSrLiH_2O_2$. *Electrochemistry* **85**, 88–92 (2017).
27. Kawaguchi, S. et al. High-throughput powder diffraction measurement system consisting of multiple MYTHEN detectors at beamline BL02B2 of SPring-8. *Rev. Sci. Instrum.* **88**, 085111 (2017).
28. Izumi, F. & Momma, K. Three-dimensional visualization in powder diffraction. *Solid State Phenom.* **130**, 15–20 (2007).
29. Oishi, R. et al. Rietveld analysis software for J-PARC. *Nucl. Instrum. Methods Phys. Res. A* **600**, 94–96 (2009).
30. Momma, K. & Izumi, F. VESTA 3 for three-dimensional visualization of crystal, volumetric and morphology data. *J. Appl. Crystallogr.* **44**, 1272–1276 (2011).
31. Frick, B., Mamontov, E., van Eijck, L. & Seydel, T. Recent backscattering instrument developments at the ILL and SNS. *Z. Phys. Chem.* **224**, 33–60 (2010).
32. Kobayashi, G., Laurent, B., Bresser, D., Bernhard, F. & Sandrine, L. Study on the dynamics of hydride ion conduction in oxyhydrides. *Institut Laue-Langevin (ILL)* https://doi.org/10.5291/ILL-DATA.7-03-144 (2016).
33. Frick, B., Combet, J. & van Eijck, L. New possibilities with inelastic fixed window scans and linear motor Doppler drives on high resolution neutron backscattering spectrometers. *Nucl. Instrum. Methods Phys. Res. A* **669**, 7–13 (2012).

Acknowledgements

This work was supported by the Precursory Research for Embryonic Science and Technology programme of the Japan Science and Technology Agency, no. JPMJPR1295 (G.K.); Grants-in-Aid nos 15H05497 (G.K.), 17H05492 (G.K.), 17H06145 (R.K.), 18H05516 (G.K.), 18H05518 (T.O.), 19H04710 (F.T.) and 20H02828 (G.K.) from the Japan Society for the Promotion of Science; and the Advanced Research Program for Energy and Environment Technologies from the New Energy and Industrial Technology Development Organization, no. 16823906 (R.K.). Synchrotron and neutron radiation experiments were approved by the Japan Synchrotron Radiation Research Institute (2016A1673, 2016B1767 and 2018B1099), the Neutron Scattering Program Advisory Committee of the Institute of Materials Structure Science, the High Energy Accelerator Research Organization (2014S06, 2014S10 and 2019S10) and the Institut Laue-Langevin (http://doi.ill.fr/10.5291/ILL-DATA.7-03-144). Electrochemical impedance spectroscopy measurements were supported by N. Higuchi (Toyo Corporation). The authors thank T. Yamamoto and T. Broux for their helpful suggestions regarding structural refinement. D.B. acknowledges the NanoSciences Programme of the Atomic Energy Commission (CEA, France) and the EU/CEA Enhanced Eurotalents Fellowship for financial support.

Author contributions

G.K. conceived, supervised and designed the whole study. A.W., Y.I. and M.N. synthesized the material. F.T., A.W., K.O. and Y.I. carried out the electrochemical measurements. F.T., A.W., A.A., M.Y., T.S., K.I., T.O., T.K. and G.K. collected and refined the powder SXRD and ND data. D.B., S.L., B.F. and G.K. conducted the neutron quasi-elastic measurements and analysis. All authors discussed the results; F.T. and G.K. wrote the manuscript with discussions mainly with S.L., D.B., B.F. and R.K.

Competing interests

The authors declare no competing interests.

Additional information

Correspondence and requests for materials should be addressed to Genki Kobayashi.